Viscoelastic Contrast and Kinetic Frustration during Poly(ethylene oxide) Crystallization in a Homopolymer and a Triblock Copolymer. Comparison of Ultrasonic and Low-Frequency Rheology

I. Alig* and S. Tadjbakhsch

Deutsches Kunststoff-Institut, Schlossgartenstrasse 6, D-64289 Darmstadt, Germany

G. Floudas

Foundation for Research and Technology-Hellas (FORTH), Institute of Electronic Structure and Laser, P.O.Box 1527, 71110 Heraklion, Crete, Greece

C. Tsitsilianis

Department of Chemical Engineering, University of Patras, 26500 Patras, and Institute of Chemical Engineering and High-Temperature Processes, P.O. Box 1414, 26500 Patras, Greece

Received March 17, 1998; Revised Manuscript Received July 13, 1998

ABSTRACT: We report a combined study using an ultrasonic shear wave reflection technique and conventional low-frequency rheology for the investigation of the crystallization kinetics and melting of a poly(ethylene oxide) (PEO) homopolymer and a poly(ethylene oxide)−polystyrene−poly(ethylene oxide) (PEO−PS−PEO) triblock copolymer. Both isochronal heating and isothermal/isochronal kinetic measurements of the complex dynamic shear modulus G^* have been performed with high-frequency (ultrasonic) and conventional low-frequency rheology at frequencies of 3.5 MHz and 0.16 Hz, respectively. The different frequencies create a different viscoelastic contrast between the two phases in the two experiments. In both experiments the system can be regarded as a composite material made of spherulites within the amorphous matrix, and the increase of the shear modulus with time is attributed to the growing of spherulites at the expense of the amorphous matrix. The kinetics of crystallization are analyzed in the framework of the Avrami equation using different mechanical models that describe a two-phase composite. Although a simple parallel model composed of an amorphous and a spherulitic phase suffices to describe the ultrasonic shear experiment, a more complex model involving phase inversion is required to account for the abrupt dependence of the shear modulus on time in rheology. The effect of external shear is to speed up the kinetics. The ultrasonic shear experiments for the homopolymer crystallization are compared with those of the triblock copolymer, and it is found that the final modulus in the latter is considerably lower than that in the former experiment. This is explained by the less perfect structure of the lamellae and/or the spherulites in the copolymer and the kinetic frustration of the crystallization (for low undercooling) due to the glassy PS microphase. It is shown that the comparison of high and low-frequency rheology can provide new insights on the crystallization process and the final morphology in semicrystalline polymers.

Introduction

The investigation of crystallization and melting has attracted many researchers for about sixty years.[1,2] Among those studies there is a large number of investigations on the crystallization in macromolecular systems (see, e.g., refs 3−5). Besides its importance for the processing of semicrystalline polymeric materials, the question of polymer crystallization is still of large fundamental importance. This is especially the case since the chain connectivity, the related high viscosity of polymers, and entanglements of polymer chains influence the crystallization kinetics and the final morphology of semicrystalline polymer materials. The morphology as well as the crystallization kinetics and melting behavior has been studied extensively by light and electron microscopy, X-ray scattering and calorimetry.[4] Despite the large importance in understanding the processing of semicrystalline polymers (for example, during injection moulding), there are very few experimental investigations[5−7] of the effect of applied shear on polymer crystallization.

Another aspect of polymer crystallization is the influence of chain architecture on the crystallization and final morphology. Block copolymers composed of crystalline and amorphous blocks are suitable materials for such investigations (see refs 7−18). In a very recent paper, some of us[7] reported on the structure and dynamics of structure formation in poly(ethylene oxide) (PEO) and in two triblock copolymers of poly(ethylene oxide)−polystyrene−poly(ethylene oxide) (PEO−PS−PEO) using rheology and calorimetry. Although the characteristic times from the both experiments where comparable, there was a pronounced effect of the shear field on the time dependence of the crystallization process. An ideal investigation of the effect of shear on the viscoelastic properties of crystallizable systems requires a comparison of exactly the same properties (i.e., moduli) measured under nondestructive conditions.

In previous papers[19−21] we reported on a shear wave reflection technique in the ultrasonic frequency range for time- and temperature-dependent measurements of the complex dynamic shear modulus ($G^* = G' + iG''$) as well as on its application for monitoring time-dependent isothermal processes or reactions. This

* To whom the correspondence should be addressed.

S0024-9297(98)00420-3 CCC: $15.00
Published on Web 09/15/1998

Table 1. Molecular Characteristics of the PEO and the PEO−PS−PEO Triblock Copolymer

sample	$\bar{M}_w$	$\bar{M}_w/\bar{M}_n$	$\bar{M}_w$(PS)	$\bar{M}_w/\bar{M}_n$ (PS)	$\bar{M}_w$(PEO block)	W_{PS} (%)	X_c^{WAXS} (%)	X_c^{DSC} (%)
PEO-35	35 000	1.15				0	64	70
ESE-2	82 000	1.17	33 500	1.13	24 200	34		52

method supplies the viscoelastic properties in films with free surfaces. Few applications of the method have already been reported. For example, the film formation of dispersions[19,20] and the associated crystallization kinetics have been investigated.[19] Furthermore, we reported on the applicability of the method for temperature-dependent measurements of melting and recrystallization in a semicrystalline polychloroprene sample.[19,20] In a very recent study[21] we showed the agreement between the ultrasonic shear and low-frequency rheological experiments in an amorphous polymer with respect to the glass−rubber relaxation.

In this work we present the first detailed comparison of the crystallization kinetics and melting by employing conventional low-frequency rheology and ultrasonic shear (a nondestructive technique) on identical samples. With these techniques we are able to extract and compare directly the same viscoelastic properties of the semicrystalline PEO in the homopolymer and in the triblock copolymer PEO−PS−PEO. The copolymer was identical to one of the samples studied before.[7] The samples have been characterized by X-ray scattering, differential scanning calorimetry (DSC), and polarization microscopy.

In both experiments the influence of crystallization on the dynamic shear modulus was studied by employing the Avrami equation[2] on a two-phase system composed of spherulites in an amorphous matrix. We have developed a mixing rule for the shear wave reflection coefficient and compare it with mixing rules for the moduli. We found that the ultrasonic shear modulus could be described by a parallel mixing law of the two phases. However, the crystallization kinetics in the rheological experiments could not be described in the framework of a simple mixing law. Different mechanical models have been employed and compared. There are pronounced differences in the crystallization time dependence of the modulus as probed by the two experiments, which are attributed to (i) different mixing laws of a two-phase system and (ii) to the external shear applied only in conventional rheology. The glassy midblock in the triblock copolymer introduces a competition between the thermodynamic driving forces favoring crystallization with the hindered mobility of PEO chains introducing structural defects.

II. Experimental Section

Materials. The synthesis of the PEO−PS−PEO was described before.[7] All samples were characterized by size exclusion chromatography, light scattering, differential refractometry and elementary analysis. The structure and crystallization kinetics have been studied by differential scanning calorimetry (DSC) and X-ray scattering. Details of the results from DSC and X-ray scattering have been reported earlier.[7] The molecular characteristics of the samples are given in Table 1.

Shear Wave Reflection Method. A schematic drawing of the shear wave reflection cell is shown in Figure 1. An ultrasonic shear wave is transmitted into a fused quartz glass bar by means of an AT-cut quartz transducer (T_1). The shear wave is reflected off the quartz bar/sample interface and is then detected by a second transducer (T_2) at the other end. To avoid mode transformation at the reflecting surface, the transducer must be oriented in such a way that the particle motion of the shear wave is parallel to the surface. Under these conditions the complex shear impedance (Z^*) of the viscoelastic sample can be determined from the absolute value of the reflection coefficient (r) and the phase shift (δ) caused by the sample (see ref 2 in ref 19 and ref 1 in ref 20). Assuming that the shear mechanical impedance of the quartz bar (Z_q) has only a real component, Z^* can be expressed by

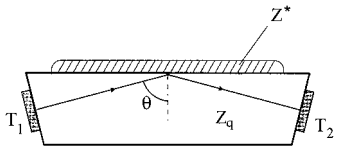

Figure 1. Schematic drawing of the sample cell of the shear wave reflection method. Z_q and Z^* are the shear mechanical impedances of the fused quartz rod and the viscoelastic film, respectively. T_1 and T_2 are the transmitting and receiving transducers. The angle θ is explained in the text.

$$Z^* = R + iX = Z_q \cos\theta \frac{1 - r^2 + 2ir\sin\delta}{1 + r^2 + 2r\cos\delta} \quad (1)$$

and

$$r = \left(\frac{A_1}{A_0}\right)^{1/(2n-1)} \quad (2)$$

where A_1 and A_0 are the amplitudes of the nth echo with and without sample, respectively. To obtain an enhanced experimental effect, θ was chosen to be 79°. Since δ is very sensitive to the temperature of the sample cell, the ultrasonic unit is kept in a temperature stability of 0.02 K. Details of the experimental setup are described elsewhere.[19,20]

The complex shear modulus G^* of the sample is related to the shear impedance Z^* by

$$G^* = G' + iG'' = \frac{(Z^*)^2}{\rho} \quad (3)$$

where ρ is the density of the sample. Then the storage modulus G' and the loss modulus G'' are given by

$$G' = \frac{R^2 - X^2}{\rho} \quad (4)$$

and

$$G'' = \frac{2RX}{\rho} \quad (5)$$

It is noteworthy that the shear modulus in viscoelastic materials depends on the ultrasonic frequency. All measurements presented here were performed at the fixed frequency of 3.5 MHz ($f = \omega/2\pi$).

Rheology. The low-frequency measurements of the storage (G') and the loss (G'') modulus were made with a Rheometric Scientific dynamic stress rheometer (DSR) with a controlled strain option in a parallel plate geometry (with a plate separation of 0.5 mm) within the frequency range from $10^{-1} < \omega < 10^2$ rad/s. The isochronal crystallization experiments were made at 1 rad/s ($f = 0.16$ Hz). The temperature control was better than 0.1 K. Details of the experimental setup can be found in ref 7.

III. Results and Discussion

PEO Homopolymer. PEO is known to be a very sensitive probe of crystallization;[22−25] therefore we have

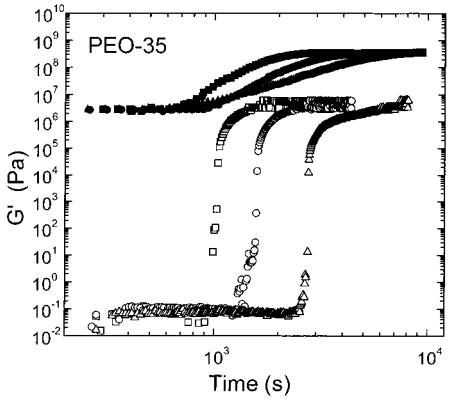

Figure 2. Comparison of time dependence of the storage modulus $G'(t)$ measured by the ultrasonic shear wave reflection technique (filled symbols) and rheology (open symbols) during isothermal crystallization of PEO for representative crystallization temperatures, T_c. The sample was initially heated above its melting temperature and quenched to different final temperatures: (□, ■) 56 °C; (○, ●) 57 °C; (△, ▲) 58 °C.

chosen this polymer to compare the results of the ultrasonic shear wave reflection method with rheology and to investigate the effect of shear on crystallization. Representative examples of isothermal crystallization experiments after quenches from $T > T_m^\circ$ (T_m° is the equilibrium melting temperature) to different crystallization temperatures, T_c, with both methods are shown in Figure 2. The short- and long-time plateau values are associated, respectively, with the undercooled melt and the semicrystalline material (space filling-spherulitic structure). Large differences between the limiting moduli $G'(\omega, t = 0)$ and $G'(\omega, t \rightarrow \infty)$ for the ultrasonic experiments at $\omega_{us} = 2\pi f_{us}$ and for the rheological measurements at a lower frequency ($\omega_{rh} = 2\pi f_{rh}$) are evident. The initial modulus ($t = 0$) of the undercooled homopolymer is $G'_{PEO}(\omega_{us}, t = 0) = 3$ MPa at the ultrasonic frequency $f_{us} = 3.5$ MHz, and $G'_{PEO}(\omega_{rh}, t = 0) = 1 \times 10^{-1}$ Pa at the much lower rheological frequency $f_{rh} = 0.16$ Hz. The final moduli ($t \rightarrow \infty$) are nearly independent of the undercooling ($T_m^\circ - T_c$) in both methods with the limiting values of G' of 350 and 10 MPa for the "ultrasonic" and conventional rheology, respectively. The differences in the moduli in the melt state as well as the separation of the moduli between the initial and the final states, in the two experiments, can be qualitatively explained by Scheme 1a. In the scheme, the frequency dependence of the storage modulus for undercooled (or amorphous) melts is compared with that of a semicrystalline homopolymer. The characteristic frequencies in the two experiments are indicated by ω_{rh} and ω_{us} and the increase of $G'(t)$ during the isochronal experiments is indicated by arrows. At the frequency of the ultrasonic shear experiment (ω_{us}) the amorphous melt is characterized by a shear modulus that is typical for the rubbery plateau. During crystallization, part of the amorphous component is converted to crystalline lamellae and the sample is finally completely space-filled by spherulites. Therefore the modulus of the final semicrystalline material can be described by a kind of a mixing law. A model for the modulus of a spherulite is given by Halpin and Kardos.[26]

At the frequency of the rheological experiment (ω_{rh}), the shear modulus of the undercooled amorphous melt corresponds to the flow region characterized by $G' \propto \omega^2$. During the crystallization process, part of the amorphous matrix is converted to spherulites and the final modulus characterizes a semicrystalline material at ω_{rh} (see arrow in Scheme 1a). It is because of the low shear modulus at $t = 0$ that the step in $G'(t)$ is much more pronounced in rheology than in the ultrasonic experiment. As we will discuss below, the different frequencies involved in the two experiments create the different viscoelastic contrasts between the initial and final states.

Scheme 1

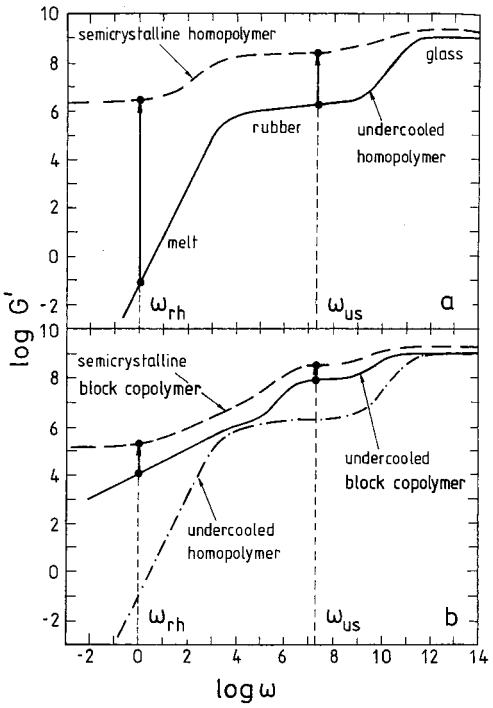

In the analysis of the isochronal/isothermal kinetic experiments, we have assumed a nucleation and growth mechanism and suitable mechanical models to describe the transformation (incorporation) of the amorphous matrix to the spherulitic structure. A combination of the Avrami equation[2] with a "series" or "parallel" model for a two-phase composite made of an ordered and disordered phase has been applied by Floudas et al.[27] to the ordering kinetics of amorphous block copolymers and was recently extended to the crystallization process in semicrystalline/amorphous block copolymers.[7] The time dependence of the volume fraction of the crystalline component ϕ_c during isothermal crystallization can be expressed by the Avrami equation[2]

$$\phi_c = 1 - \exp(-kt^n) \qquad (6)$$

where n is the Avrami exponent and k is a rate constant. The Avrami exponent reflects the dimensionality of the growth and the nature of the nucleation and growth process. A value of $n = 4$ is proposed for spherulite growth and homogeneous nucleation, whereas a value of $n = 3$ can result from spherulitic growth with heterogeneous nucleation or lamella growth with homogeneous nucleation.[4]

In a simplified model a semicrystalline polymer can be considered as a composite of an amorphous and a crystalline phase. Another model would be to assume an amorphous phase and the spherulites as the second component. The latter is again a composite of the crystalline lamella and the unconverted amorphous

Scheme 2

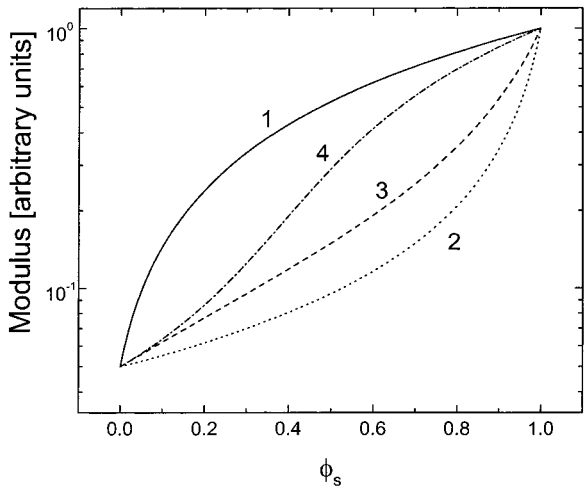

phase within the spherulite. Since in the final state the system is fully space-filled by the spherulites, it is reasonable to assume that the two-phase system is composed of spherulites and an amorphous phase. The upper and lower bounds for the volume fraction dependence of the composite modulus G^* are given by a "parallel" model (Voigt)

$$G^* = (1 - \phi_S)G_a^* + \phi_S G_S^* \tag{7}$$

and by a "series" model (Reuss)

$$1/G^* = (1 - \phi_S)/G_a^* + \phi_S/G_S^* \tag{8}$$

respectively, where ϕ_s is the volume fraction of spherulites and G_a^* and G_S^* are the shear moduli of the amorphous and spherulitic phases, respectively. Assuming a constant ratio of amorphous to crystalline component inside the spherulite during its growth, ϕ_c in eq 6 can be replaced by ϕ_S for the data analysis in the framework of this simple model.

To visualize the different ϕ_S dependencies for different mixing models, the curves for the real part of shear modulus calculated with the series (dotted line, 2) and parallel (solid line, 1) models are shown in Scheme 2. The properties of a composite of any two phase geometry must lie between the two limits. For spherical particles included in a matrix, the Kerner model[28] can be applied. According to this model the modulus of the composite is given by

$$G^* = G_a^* \frac{\phi_a G_a^* + (\gamma + \phi_S)G_S^*}{(1 + \gamma\phi_S)G_a^* + \gamma\phi_a G_S^*} \tag{9}$$

where $\gamma = 2(4 - 5\nu)/(7 - 5\nu)$ and ν is Poisson's ratio of the composite. The result for G' from the Kerner model is also shown in Scheme 2 (dashed line, 3) and is intermediate between the series and parallel model. A model that predicts phase inversion at intermediate compositions was developed by Budiansky:[29]

$$\frac{\phi_a}{1 + \epsilon\left(\frac{G_a^*}{G^*} - 1\right)} + \frac{\phi_S}{1 + \epsilon\left(\frac{G_S^*}{G^*} - 1\right)} = 1 \tag{10}$$

where $\epsilon = 2(4 - 5\nu)/15(1 - \nu)$. As shown in Scheme 2 (dashed-dotted line, 4), this model yields a drastic change in the mixing law over the small ϕ_S range of the phase inversion.

In the ultrasonic shear experiment the specific limitations of the different mixing laws have to be considered more in detail since the wavelength λ, of the ultrasonic shear wave is much smaller (in the range from 15 to 160 μm) than the "wavelength" of the rheological experiment (in the range from 7 cm to 300 m). When the ultrasonic wavelength λ is bigger than the spherulite size, the Kerner model is well suited for describing the shear modulus of the composite. This was shown recently for the crystallization in a semicrystalline polychloroprene by ultrasonic shear experiments.[30] For the PEO considered here the situation is different, since the spherulitic radius exceeds the sound wavelength after the initial period of crystallization and the reflected shear wave is not sensitive to the geometrical shape of spherulites. Since the ultrasonic technique operates in the reflection mode, a mixing law applies to the reflection coefficient $r^* = r \exp(-i\delta)$ rather than to the moduli of the phases:

$$r^* = (1 - \phi_S)r_a^* + \phi_S r_S^* \tag{11}$$

r_a^* and r_S^* are the reflection coefficients for the amorphous phase ($r_a = 0.975$) and the spherulite ($r_S = 0.465$), respectively. Using $Z^*/Z_q = (1 - r^*)/(1 + r^*)$ and eq 3, we get the following expression for the complex shear modulus:

$$G^* = \frac{Z_q^{\,2}}{\rho}\cos^2\theta\left(\frac{1 - r^*}{1 + r^*}\right)^2 \tag{12}$$

Since the measured phase shifts δ_a and δ_S do not exceed 0.06 rad, the real part of the shear modulus can be approximated ($\cos\delta \approx 1$ and $\sin\delta \approx 0$) as

$$G' = \frac{Z_q^{\,2}}{\rho}\cos^2\theta\frac{(1 - r^2)^2}{(1 + r^2 + 2r)^2} \tag{13}$$

As we will show below with respect to Figure 3, this "parallel" mixing law for the reflection coefficient is, within the experimental error, equivalent to a "parallel" law applied for the shear modulus (eq 7).

In Figure 3 we compare the measured $G'(t)$ from high-frequency (ultrasonic) and low-frequency rheological experiments, at 58 °C, with the different models discussed above by incorporating the Avrami dependence for ϕ_S with $n = 3$ and $k = 4.1 \times 10^{-12}$ s^{-3} (the latter parameters were obtained from the fits to the ultrasonic data; see below). For the parameters G_a' and G_S' the respective values of $G'(t)$ at $t = 0$ and $t \to \infty$ were used. The ultrasonic $G'(t)$ values can be well represented by the "parallel" model for the reflection coefficient (dash-double dotted line of Figure 3) and the parameters are given in Table 2. This is reasonable, since the crystallization process is rather fast so that the size of the spherulites soon exceeds the ultrasonic wavelength. In the error limits this fit is almost equivalent to a fit using a parallel model for the moduli (see eq 7 and Figure 3). For the rheological data a fit using the "parallel" or "series" models with reasonable Avrami parameters is not possible. The solid and dotted lines in Figure 3 are the result of the "parallel" and "series" models, respectively, using the n and k values from the ultrasonic data. The Kerner model is also not directly applicable in both data sets, as shown by the dashed lines in Figure 3 (n

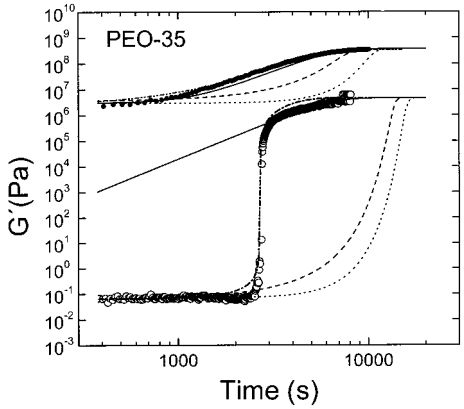

Figure 3. Comparison of the time dependence of the storage modulus G' measured by the ultrasonic shear wave reflection technique (●) and rheology (○) during isothermal crystallization of PEO with $T_c = 58$ °C. The solid and dotted curves are calculated for the "parallel " and "series" model incorporating an Avrami-type dependence for ϕ_S with $n = 3$ and $k = 4.1 \times 10^{-12}$. The dashed line is calculated from the Kerner model, and the dash-double dotted line, from the "parallel" model for the reflection coefficient using the same Avrami parameters. The dashed−dotted line represents a direct fit for the Budiansky model incorporating the Avrami equation to the low-frequency data, which results in different Avrami parameters (see text).

Table 2. Parameters of the Data Analysis of the Isothermal Ultrasonic Crystallization Experiments of PEO and the PEO−PS−PEO Triblock Copolymer[a]

sample	T_c (°C)	G_a (MPa)[b]	G_s (MPa)	k (s^{-n})	n	$t_{1/2}$ (s)[c]
PEO-35	53	3	367	9.9×10^{-10}	3.1	760
	54	3	361	5.2×10^{-10}	3.1	940
	55	3	352	2.78×10^{-10}	3.1	1125
	56	3	352	8.4×10^{-11}	3.1	1510
	57	3	348	3.7×10^{-12}	3.3	2870
	58	3	339	4.1×10^{-12}	3.0	5370
ESE-2	(48)	85	(313)	(1.0×10^{-9})	(3.1)	(742)
	(49)	85	(290)	(4.7×10^{-10})	(3.2)	(800)
	(49.5)	85	(280)	(2.5×10^{-10})	(3.0)	(1400)
	50	85	268	1.7×10^{-10}	3.0	1520
	50.5	85	251	6.5×10^{-11}	3.0	2090
	51.5	85	225	1.1×10^{-11}	3.1	3475
	52	85	198	6.0×10^{-12}	2.9	6145
	53	85	156	9.4×10^{-12}	2.8	8950

[a] The experimental data for G' are fitted by using a combination of a parallel model for the reflection coefficient (eq 13) and the Avrami equation (eq 6) as described in the text. The parameters are in the error limit equivalent to a fit to the parallel model for the shear moduli (eq 7). [b] Fixed to the experimental value for $G'(t = 0)$. [c] $t_{1/2} = (\ln 2/k)^{1/n}$.

and k values from the ultrasonic data). The tremendous change in $G'(\omega_{rh}, t)$, which results from the large viscoelastic contrast of the amorphous and spherulitic phases at the ω_{rh}, can be coupled with a percolation-like change in the morphology over a small ϕ_S range, which is implicit to the Budiansky model. In contrast to the series, parallel, and Kerner models, for the Budiansky model a direct fit to the low-frequency data (dashed−dotted line) is shown in Figure 3, which results in different parameters for n and k ($k = 2.8 \times 10^{-10}$, $n = 2.7$, $\epsilon = 0.4$). This percolation-like change of the modulus can be attributed to a phase inversion, from spherulites in an amorphous matrix to an amoprhous phase within a crystalline matrix. In addition, the confined geometry of the rheometer plates may result in a "percolation path" of the crystalline lamellae inside the spherulites when the size of the spherulites (in the polarization microscopy spherulites up to 2 mm diameter have been found) becomes comparable to the gap (0.5 mm).

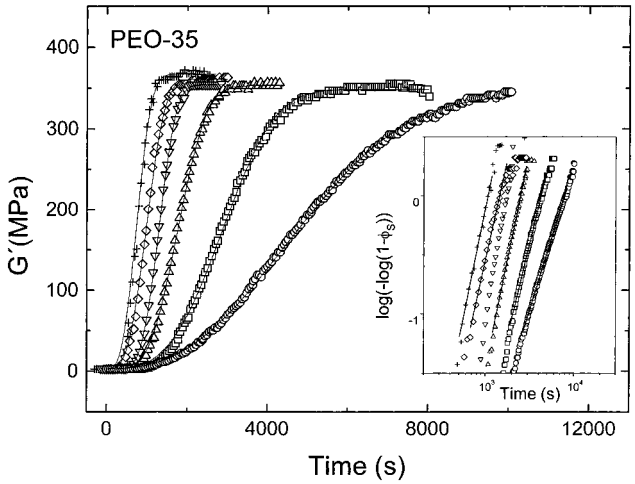

Figure 4. Isothermal crystallization of PEO measured by ultrasonic shear after quenches to different crystallization temperatures, T_c: (+) 53 °C; (◇) 54 °C; (▽) 55 °C; (△) 56 °C; (□) 57 °C; (○) 58 °C. The solid lines represent the fit by a combination of a "parallel" model for $G'(t)$ and the Avrami equation (see text). In the inset, the volume fraction of spherulites is plotted in the usual representation and fitted to the Avrami equation.

In the rheological experiment we cannot exclude the possibility of shear-induced nucleation. External shear is known to affect the crystallization process in semicrystalline polymers.[5] The increase of crystallinity during shearing has been attributed to an increasing number of nuclei rather than to the increase in the growth rate of the existing nuclei. Based on this experimental finding, models have been developed to describe the fast process of shear-induced nucleation as a function of the shear rate ($d\gamma/dt$) and the shearing time (t_s).[5] The number of nuclei per unit volume was found to scale as $(d\gamma/dt)^2 t_s$, but the values of $d\gamma/dt$ were much higher than the ones used in our rheological experiment ($d\gamma/dt \sim 0.16\ s^{-1}$).

The fits to the ultrasonic shear wave data $G'(t)$ during isothermal crystallization with the "parallel" model for the reflection coefficient (eq 11) together with eq 6 (where ϕ_c is replaced by ϕ_S) are shown by the solid lines in Figure 4, and the corresponding parameters are summarized in Table 2. As an alternative to fitting the $G'(t)$ curves, the volume fraction ϕ_S of the spherulites can be calculated by using the "parallel" model, by $\phi_S(t) = [G^*(t) - G_a^*]/[G_S^* - G_a^*]$. The $\phi_S(t)$ data are then fitted by eq 6 in the linear region in a $\log[-\log(1 - \phi_S)]$ versus $\log t$ plot, as shown in the inset to Figure 4. The half-times of crystallization estimated from this procedure are again in agreement with the ones given in Table 2.

In Figure 5 the characteristic crystallization times ($t_{1/2}$) from the two experiments are compared at some crystallization temperatures. As shown, the half-times $t_{1/2}$ of the ultrasonic experiments are somewhat longer (by a factor of 2) than those for the rheological experiments for the same crystallization temperature, which again reflects a somewhat faster crystallization due to the macroscopic shear in the latter experiment. To emphasize the very different shapes of crystallization, the reduced shear moduli ($G'_{nor}(t) = [G'(t) - G_S]/[G'_S - G'_a]$) for "ultrasonic" and conventional rheology $G'(t)$

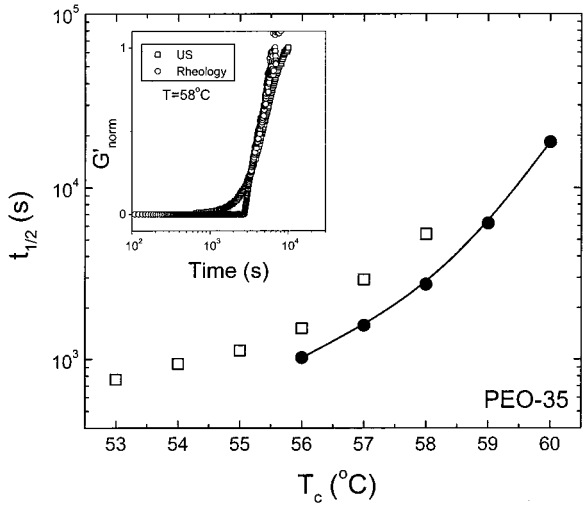

Figure 5. Half-times for the isothermal crystallization process of PEO measured by ultrasonic shear (□) and rheology (●) as a function of the crystallization temperature T_c. The line through the rheological times is a guide to the eye. The inset shows the comparison of the reduced shear moduli from high- (ultrasonic) and low-frequency rheology at the same crystallization temperature T_c = 58 °C.

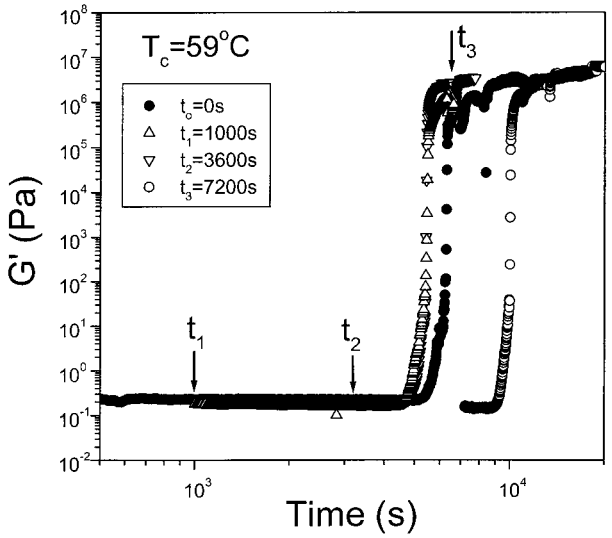

Figure 6. Influence of macroscopic shear on the crystallization kinetics of PEO at 59 °C. The experiment is made with continuous shear (delay t_0 = 0 s) and for different waiting times during which the shear field was switched off: t_1 = 1000 s, t_2 = 3600 s, and t_3 = 7200 s.

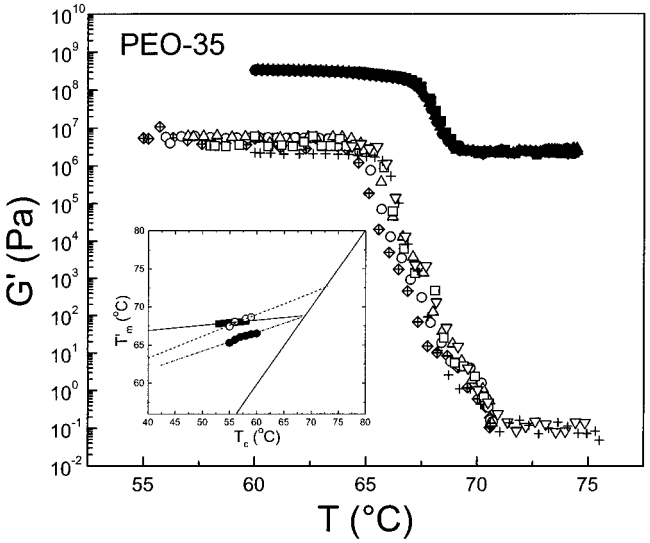

Figure 7. Comparison of the temperature dependence of the storage modulus G' obtained from ultrasonic shear (filled symbols) and rheology (open symbols) during heating after the isothermal crystallization of PEO at different temperatures: (◇) T_c = 55 °C; (○) T_c = 56 °C; (△) T_c = 57 °C; (□) T_c = 58 °C; (▽) T_c = 59 °C; (+) T_c = 60 °C. In the inset, the Hoffman–Weeks plot used to obtain the equilibrium melting temperature is shown from the high- (■) and low-frequency rheological ($T_{m,1}$ (●), $T_{m,2}$ (○)) experiments.

are compared, in the inset to Figure 5, at the same crystallization temperature (T_c = 58 °C). It is evident that the ultrasonic data follow an S-shaped curve typical of an Avrami process, whereas the rheological data seem to have an "induction" period after which an extremely steep increase in the modulus (more than 5 orders of magnitude) occurs. However, within the context of the Budiansky model, which fits well to the experimental data, at the end of the long "induction" time about 30% of the material is composed from spherulites.

To investigate the influence of macroscopic shear on the crystallization kinetics, we have made a separate rheological experiment where the shear field was switched-off for different delay intervals of time t (t_1 = 1000 s, t_2 = 3600 s, and t_3 = 7200 s) after the crystallization temperature at 59 °C was reached. The corresponding $G'(t)$ are plotted in Figure 6 and compared with the t_0 = 0 s measurement where shear is applied continuously while cooling the sample to T_c and during the crystallization process. For short delay times (t_1 = 1000 s and t_2 = 3600 s) there is only a minor shift of the curves toward a shorter time, which is probably caused by the slightly different final temperature. Thus, for short delay times there is practically no effect of the external shear. However, a large effect is observed for the longer delay time (t_3 = 7200 s). For such delay times the effect of continuous shear is to speed-up the crystallization process by a factor of 2. Therefore, the external shear interferes with the crystallization process. Notice that it is the latter experiment (long delay times) that approximates better the conditions of the nondestructive ultrasonic experiment. In this context, we should note that using long delay times the characteristic crystallization times, $t_{1/2}$, from the two experiments (plotted in Figure 5) can be brought to coincidence. This situation for PEO can be contrasted with the rheological response of amorphous block copolymers during the ordering process. In such materials we have shown[31] that switching-off the shear field does not interfere with the ordering process. We should note, however, the smaller viscoelastic contrast between the disordered and ordered states in these materials ($G'(t)$ increase by 1−2 orders of magnitude) as compared to the amorphous and spherulitic states of semicrystalline materials.

At the end of the isothermal crystallization experiments, isochronal heating runs have been performed in both experiments, aiming to obtain the apparent melting temperatures T'_m and subsequently the equilibrium melting temperatures, T°_m. T'_m was determined from the $G'(T)$ curves in Figure 7 as the temperature at midrange of the transition, which is identical to the minimum in (dG'/dT). The results for both methods are compared in Figure 7. For the ultrasonic shear experiments a single step ($T'_{m,us}$), could be resolved. In the rheological melting experiments, there are two steps that might reflect the melting of different lamellar

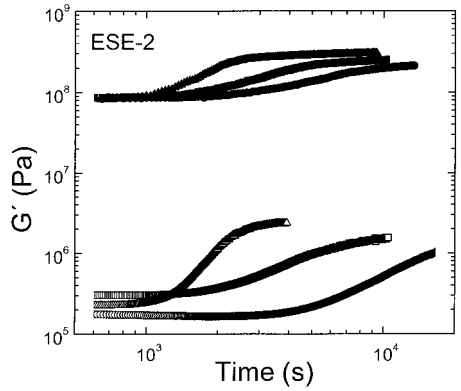

Figure 8. Comparison of the time dependence of the storage modulus G' measured by ultrasonic shear (filled symbols) and rheology (open symbols) during the isothermal crystallization of a PEO−PS−PEO triblock copolymer (ESE-2). Data at some representative temperatures of crystallization are shown: (▲, △) 50 °C; (■, □) 51 °C; (●, ○) 52 °C.

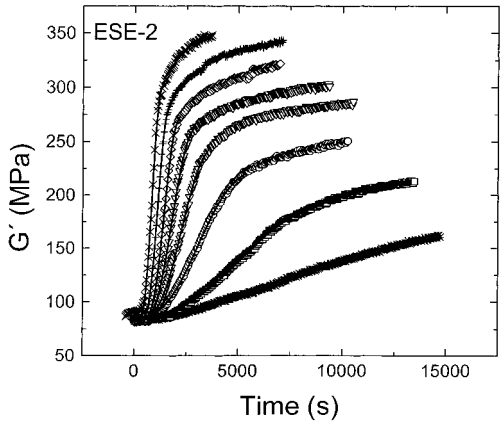

Figure 9. Isothermal crystallization of the ESE-2 triblock copolymer after quenches to different crystallization temperatures T_c: (×) 48 °C; (+) 49 °C; (▽) 50 °C; (△) 50.5 °C; (○) 51.5 °C; (□) 52 °C; (∗) 53 °C.

structures, indicated by T'_{m,rh_1} and T'_{m,rh_2}. The T'_m values in the high- and low-frequency rheological experiments are summarized in the Hoffman−Weeks plot (inset to Figure 7) and the "equilibrium" melting temperatures for the different methods ($T°_{m,us}$, $T°_{m,rh_1}$, $T°_{m,rh_2}$) are obtained by the usual extrapolation to the line $T'_m = T_c$. It is worth noting that the ultrasonic ($T°_{m,us}$) and the lower equilibrium melting temperature ($T°_{m,rh_1}$) from rheology (larger step in $G'(T)$) are very similar. The difference in the equilibrium melting temperatures may originate from the different heating rates (rheology, 1 K/min; ultrasonic, 20 K/h) involved in the two experiments.

PEO−PS−PEO Triblock Copolymer. Based on the X-ray and calorimetric studies,[7] the glassy midblock exerts a strong influence on the structure and crystallization process of the triblock copolymer. The crystallization starts from the microphase-separated state and the consequences from the presence of the PS on the structure are (i) a reduction of $T°_m$ and (ii) a decrease in the degree of crystallinity (Table 1) and crystal thickness. This structural information will be used later with respect to Scheme 1b. Here we compare the results of the isothermal crystallization experiments for both high- and low-frequency rheological experiments (Figure 8), at some representative temperatures. The main difference in the $G'(t)$ with respect to the isothermal crystallization curves of PEO is that the short-time plateau, $G(\omega, t \rightarrow 0)$, is shifted upward in both experiments. The values of the shear moduli at $t = 0$ are $G'_{ESE}(\omega_{us}, t = 0) = 85$ MPa and $G'_{ESE}(\omega_{rh}, t = 0) \approx 0.2-0.4$ MPa for the ultrasonic and low-frequency rheological experiments, respectively. These values have to be compared to those of the undercooled PEO (3 MPa and 0.1 Pa, respectively). The final values, $G'_{ESE}(\omega, t \rightarrow \infty)$, are 3×10^8 Pa and 2×10^6 Pa for the high- and the low-frequency experiment, respectively.

The situation for an isochronal/isothermal crystallization experiment of an undercooled yet microphase-separated block copolymer consisting of a glassy and a crystallizable block is schematically shown in Scheme 1b. In the high-frequency range, two glass transitions related to the two microphases are indicated in the G' versus ω plot with the two steps (solid line in Scheme 1b). To illustrate the difference between the undercooled but segregated block copolymer and the homopolymer, the lower curve from Scheme 1a is also plotted (dash−dotted) in Scheme 1b. At the ultrasonic frequency, ω_{us}, the PS blocks are glassy whereas the PEO blocks are in the melt or in the rubbery state; therefore the modulus at $t = 0$ of the undercooled triblock copolymer is more than 1 order of magnitude larger than that of PEO under the same conditions. The dashed line again indicates the final modulus following isothermal crystallization at T_c. In the rheological experiment, the considerable higher starting modulus $G'(t = 0)$ of the undercooled triblock copolymer compared to those in the PEO can be easily explained by the fact that the homopolymer is in the flow region ($G' \propto \omega^2$), whereas the block copolymer is in the undercooled but microphase-separated state with a weak frequency dependence ($G' \propto G'' \propto \omega^{1/2}$).[32−35] The lower final value $G'(\omega_{rh}, t \rightarrow \infty)$ for the triblock copolymer and its dependence on undercooling (see below) may be due to a less perfect structure within the spherulites and/or the lower degree of crystallinity. The increase of $G'(t)$ during the isothermal/isochronal high- and low-frequency experiments is represented in Scheme 1b by arrows at the respective frequencies.

In Figure 9 the analysis of the kinetic ultrasonic experiments by using the "parallel" model for the reflection coefficient (eq 11) and the Avrami eq (6) are indicated by the solid lines. To identify the interval where the fits have been performed, the solid lines in Figure 9 are shown only in a limited time region. The fitting parameters are summarized together with the PEO parameters in Table 2. Since the experiments for the triblock copolymer at the lower crystallization temperatures are not strictly under isothermal conditions (see Figure 11, below), the fit parameters for the three lower crystallization temperatures in Table 2 are given in parentheses. For the apparent crystallization temperature we used the average temperature over the initial interval of crystallization where the fits have been performed.

The $G'(t)$ display a very different dependence as compared to the homopolymer and only the initial part of the kinetic curves could be fitted by the same model, as indicated by the solid lines. Comparing the G_S values obtained by the fit (see Table 2) to the values of $G'(t \rightarrow \infty)$ a lag of the fit in the long time region becomes obvious. The fit underestimate the moduli at long times. The long-time increase of the modulus reflects a slow highly restricted crystallization process and possibly a secondary crystallization. Furthermore, the

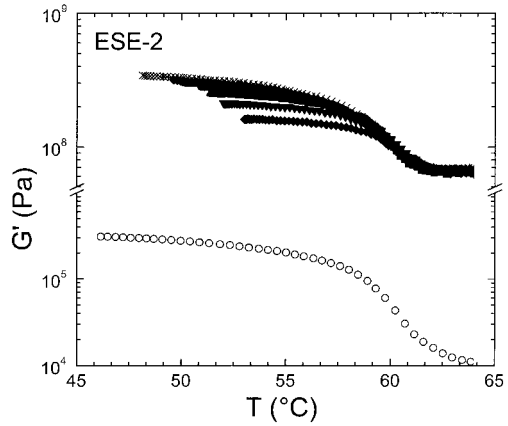

Figure 10. Comparison of the temperature dependence of the storage modulus G' obtained from ultrasonic shear [(×) 48 °C; (+) 49 °C; (◆) 49.5 °C; (□) 50 °C; (●) 50.5 °C; (▲) 51.5 °C; (▼) 52 °C; (△) 53 °C] and rheology [(○) 40 °C] during heating following the isothermal crystallization at T_c.

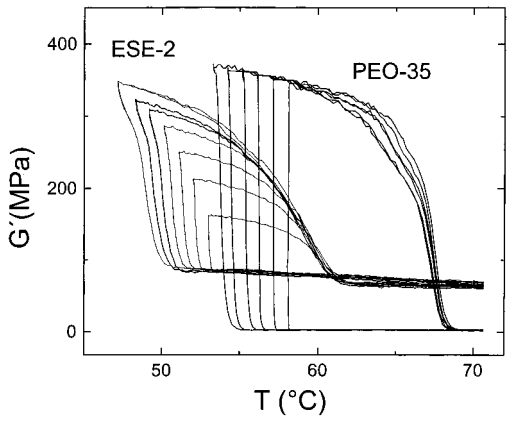

Figure 11. Composite plot showing the isochronal/isothermal crystallization measurements of G' together with the subsequent isochronal heating for the homopolymer and the triblock copolymer (ESE-2) obtained with ultrasonic shear at $f_{us} = 3.5$ MHz. The heating rate was 20 K/h.

final values of $G'(t \rightarrow \infty)$, which is identical to the spherulite modulus G_S, are a function of the undercooling and the lower the T_c, the higher the modulus. This finding will be discussed later in detail. The Avrami exponents obtained from the initial portions of the $G'(t)$ curves vary between 2.7 and 3.4, which is indicative of a three-dimensional growth mechanism from homogeneous nuclei or a two-dimensional growth from heterogeneous nuclei. Similar parameters were obtained by fitting the ϕ_S to the parallel model.

Following the crystallization experiments of the triblock copolymer, we performed isochronal heating experiments to extract the corresponding melting temperatures at the different T_c. The results from both methods are summarized in Figure 10 and will be discussed with respect to Figure 12 below.

Comparison between PEO and PEO−PS−PEO. We can now proceed in the comparison of the results for the homopolymer with the triblock copolymer. A composite plot of the ultrasonic shear experiments for the homopolymer and the triblock copolymer is shown in Figure 11. The plot contains the isochronal/isothermal kinetic studies (vertical lines) and the isochronal heating runs (heating rate: 0.33 K/min) following the crystallization kinetics. There is a clear suppression of the melting points T'_m of PEO in the triblock copolymer

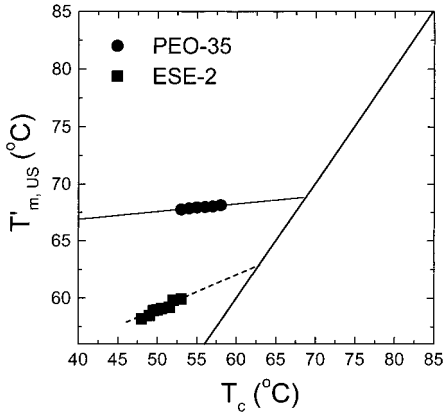

Figure 12. Hoffman−Weeks plot for PEO and the ESE-2 triblock copolymer illustrating the different values for T_m° for different experimental methods and the decrease of T_m° for the triblock copolymer.

as compared to the homopolymer. Furthermore, the differences in the moduli of the undercooled homopolymer and triblock copolymer can be clearly seen and discussed with the help of Scheme 1b. It is worth noticing that in the case of the homopolymer the final moduli are nearly identical ($G'(t \rightarrow \infty) \sim 350$ MPa) and independent of the undercooling. However, for the triblock copolymer the situation is different. For deep quenches (i.e., $T_m^\circ - T_c > 15$ K) the final values of $G'_{ESE}(t \rightarrow \infty)$ are only slightly below the corresponding values of $G'_{PEO}(t \rightarrow \infty)$, but for shallow undercooling the final modulus becomes a strong function of the crystallization temperature T_c.

The smaller step in G′ for the triblock copolymer can be explained by the less perfect crystal and/or spherulitic structure, which was inferred from the structure investigation. According to the X-ray scattering results the crystallinity and PEO crystal size is reduced in the triblock by about 20%. It is noteworthy that the moduli at $t \rightarrow \infty$, for the deeper quenches in the triblock copolymer, reflect the difference in crystallinity. The second observation, about the strong dependence of the long-time values of $G'_{ESE}(t)$ in the triblock, implies a strong T dependence of the underlying thermodynamic force that controls the crystallization. For shallow quenches, the thermodynamic driving force for crystallization, imposed to the PEO blocks, is small and the glassy PS effectively resists the rearrangements necessary for the formation of spherulites and the structure perfection. This effect is evident from the very slow crystallization kinetics shown in Figure 9, at the shallow quenches, and the low final value of G'_{ESE} reached within our experimental time scale, which is consistent with the picture of frustrated PEO crystals between the glassy PS domains. The restrictions create a higher density of defects within and over the boundaries of the spherulites, which can be considered as a frozen-in "disorder". For deeper quenches, the driving force for crystallization is so large that glassy PS domains can be rearranged to form a final state not very far away from the "equilibrium" state at the respective temperature. The restrictions to crystallization and to structure perfection by the glassy PS result from the competition between the thermodynamic driving force for crystallization (heat of fusion, surface free energy) and the chain mobility. In this picture the glassy microdomains can restrict both the formation of crystalline lamellae and their rearrangements into spherulites (with glassy inclusions).

The results of the isochronal heating experiments designed to melt the crystalline structures are shown in Figure 12, where the apparent melting temperatures from the ultrasonic experiments for the different crystallization temperatures are compared in the usual Hoffman−Weeks representation for the homopolymer and the triblock copolymer. The first observation is that there is a melting point depression in the triblock copolymer, which is in good agreement with the results from conventional rheology. The melting point depression in the triblock is attributed to crystal imperfections and/or reduced crystal size. The second observation, is the stronger $T'_m(T_c)$ dependence in the triblock, which implies that the system is further away from "equilibrium" at the given T_c due to the frozen-in disorder. As we discussed above, this is especially true for the shallow quenches. In the linear extrapolation made to obtain the equilibrium melting temperature of the triblock copolymer, we have excluded the data points corresponding to deeper quenches since the crystallization conditions were not strictly isothermal. The equilibrium melting temperatures of the homopolymer and triblock copolymer amount to 69 and 63 °C, respectively.

Last, the structural changes imposed by a glassy block can be studied in parallel with the crystallization process by SAXS and WAXS experiments. Such experiments should reveal the different crystal sizes and crystallinities at the different crystallization temperatures. These experiments are in progress.

Conclusion

The crystallization kinetics of PEO have been studied and compared in the homopolymer and in the triblock copolymer PEO−PS−PEO—where one end of the PEO blocks is frustrated by the glassy PS lamellae—with conventional low-frequency rheology and an ultrasonic shear wave reflection method. Both techniques provide the complex shear modulus. The findings can be summarized as follows:

(i) Due to the different frequencies and the corresponding wavelength involved in the two experiments, there is a different viscoelastic contrast between the amorphous and the spherulitic phase. Since the ultrasonic wavelength is much smaller than the spherulite diameter, the applicability of the same mixing law to both experiments is impossible. We proposed a simple model that includes a "parallel" mixing rule for the shear wave reflection coefficient to describe the ultrasonic data. We found that this model is equivalent to a parallel model for the moduli. However, it is impossible to describe the low-frequency rheological data in the framework of a parallel model. In the latter experiment, a more complex model that involves a phase inversion was required to describe the abrupt time dependence of the modulus during crystallization. These models were incorporated in the Avrami analysis of the crystallization kinetics.

(ii) The applied shear stress in conventional rheology was found to speed-up the crystallization process. This is supported by the shorter characteristic crystallization times in the "nondestructive" ultrasonic experiments where the shear deformation is much smaller compared to conventional rheology.

(iii) The glassy PS midblock in the PEO−PS−PEO triblock copolymer results in a strong dependence of the shear moduli on undercooling. This is explained by a competition between the driving thermodynamic forces for crystallization and the restricted molecular mobility due to the glassy domains.

Acknowledgment. This work was supported by the Alexander von Humboldt-Stiftung and the Bundesminister für Wirtschaft through the Arbeitsgemeinschaft Industrieller Forschungsvereinigungen e.V., AiF-Grant No. 10835.

References and Notes

(1) Kolmogorov, A. N. *Isv. Akad. Nauk SSSR, Otdel. Mater. i Est. Nauk* **1937**, *1*, 355
(2) Avrami, M. J. *J. Chem. Phys.* **1939**, *7*, 1103; **1940**, *8*, 212; **1941**, *9*, 177.
(3) Mandelkern, L. *Crystallization of Polymers*; McGraw-Hill, New York, 1964.
(4) Wunderlich, B. *Macromolecular Physics*; Academic Press: New York 1976; Vols. I−III.
(5) Eder, G.; Janeschitz-Kriegl, H. *Structure Development During Processing 4: Crystallization*; Meijer, H. E. H., Ed.; Material Science and Technology; Verlag Chemie: Weinheim, 1996; Vol. 18.
(6) Liedauer, S. *Int. Polym. Processing* **1993**, *8*, 3.
(7) Floudas, G.; Tsitsilianis, C. *Macromolecules* **1997**, *30*, 4381.
(8) Lotz, B.; Kovacs, A. J.; Basset, G. A.; Keller, A. *Kolloid Z. Z. Polym.* **1966**, *209*, 115.
(9) Gervais, M.; Gallot, B. *Makromol. Chem.* **1973**, *171*, 157; **1973**, *174*, 193; **1977**, *178*, 1577; **1977**, *178*, 2071; **1979**, *180*, 2041.
(10) Shimura, Y.; Hatakeyama, T. *J. Polym. Sci., Polym. Phys. Ed.* **1975**, *13*, 653.
(11) Nojima, S.; Kato, K.; Yamamoto, S.; Aschida, T. *Macromolecules* **1992**, *25*, 2237.
(12) Unger, R.; Bayer, D.; Donth, E. *Polymer* **1991**, *32*, 3305.
(13) Richardson, P. H.; Richards, R. W.; Bundell, D. J.; MacDonald, W. A.; Mills, P. *Polymer* **1995**, *36*, 3059.
(14) Lovinger, A. J.; Han, B. J.; Padden, F. J.; Mirau, P. A. *J. Polym. Sci., Polym. Phys. Ed.* **1993**, *31*, 115.
(15) Galin, M.; Mathis, A. *Macromolecules* **1981**, *14*, 677.
(16) Douzinas, K. C.; Cohen, R. E. *Macromolecules* **1992**, *25*, 5030.
(17) Rangarajan, P.; Register, R. A.; Fetters, L. J.; Bras, W.; Naylor, S.; Ryan, A. J. *Macromolecules* **1995**, *28*, 1422.
(18) Hamley, I. W.; Fairclough, J. P. A.; Ryan, A. J.; Bates, F. S.; Towns-Andrew, E. *Polymer* **1996**, *37*, 4425.
(19) Alig, I.; Lellinger, D.; Sulimma, J.; Tadjbakhsch, S. *Farbe Lacke* **1996**, *102*, 56.
(20) Alig, I.; Lellinger, D.; Sulimma, J.; Tadjbakhsch, S. *Rev. Sci. Instrum.* **1997**, *63*, 3.
(21) Alig, I.; Tadjbakhsch, S.; Zosel, A. *J. Polym. Sci., Polym. Phys. Ed.* **1998**, *36*, 1703.
(22) Godovsky, Yu. K.; Sloninsky, G. L.; Barbar, *J. Polym. Sci., Part C* **1972**, *38*, 1.
(23) Kovacs, A. J.; Gonthier, A.; Stampe, C. *J. Polym. Sci., Part C* **1975**, *50*, 283.
(24) Kovacs, A. J.; Stampe, C.; Gonthier, A. *J. Polym. Sci. Symp.* **1977**, *59*, 31.
(25) Cheng, S. Z. D.; Zhang, A.; Barley, S. J.; Cheng, J.; Hobenschuss, A.; Zschack, P. R. *Macromolecules* **1991**, *24*, 3937.
(26) Halpin, J. C.; Kardos, J. L. *J. Appl. Phys.* **1972**, *43*, 2235.
(27) Floudas, G.; Pakula, T.; Fischer, E. W.; Hadjicrhistidis, N.; Pispas, S. *Acta Polym.* **1994**, *45*, 176.
(28) Kerner, E. H. *Proc. Phys. Soc. London* **B69**, *809*, 1956.
(29) Budiansky, B. *J. Mech. Phys. Solids* **1965**, *13*, 223.
(30) Alig, I.; Tadjbakhsch, S. *J. Polym. Sci., Polym. Phys. Ed.*, in press.
(31) Floudas, G.; Hadjicrhistidis, N.; Iatrou, H.; Pakula, T.; Fischer, E. W. *Macromolecules* **1994**, *27*, 7735.
(32) Rosedale, J. H.; Bates, F. S. *Macromolecules* **1990**, *23*, 2329.
(33) Winter, H. H.; Scott, B. D.; Gronski, W.; Okamodo, S.; Hashimoto, T. *Macromolecules* **1993**, *26*, 7236.
(34) Rubinstein, M.; Obukhov, S. P. *Macromolecules* **1993**, *26*, 1740.
(35) Kawasaki, K.; Onuki, A. *Phys. Rev. A* **1990**, *42*, 366.

MA980420X